UDC 669 . 782 . 66 - 912 : 532 . 132

Flow in Si Single Crystal Growth Melts and Its Numerical Simulation

Yutaka KISHIDA*1 Masahiro TANAKA*1

Abstract

With the production of 12" silicon wafers, the flow control of silicon melt in larger crucibles became a new technical problem in the production of silicon single crystals by the Czochralski process. Facing the problem, Nippon Steel and NSC ELECTRON CORPORATION carried out observations of the changed molten liquid flow using temperature measurements with CCD images and numerical simulations based on the observations for the purpose of clarifying the flow characteristics and working out methods to control the flow. The temperature measurements made it clear that the enlarged crucibles and change in the rotation speed caused a transition of the liquid flow from an axi-symmetric flow to baroclinic waves and geostrophic turbulence. It was also clarified that the Coriolis force hitherto neglected in the 2-dimensional axi-symmetric model of the melt flow had a determining role on the flow. The temperature measurements suggested that these phenomena could be simulated by unsteady 3-dimensional numerical calculations and the authors carried out the simulation. The result well reflected the behaviors of the real melt flow, reproducing the axi-symmetric flow, the baroclinic waves and the geostrophic turbulence as well as the transition phenomena from one of them to another. Applicability of the numerical simulation to the melt of the CZ process was thus confirmed.

1. Introduction

Facing demands for scaling up of semiconductor devices and yield improvement in their manufacturing, silicon wafer producers are promoting developments for enlarging the diameter of silicon single crystals from the present 8" to 12". The 1.5 times larger crystal diameter means an increase by 3.4 times (1.5^3) in the amount of silicon melt for the crystal production. There is no difference either 8" or 12", however, in that the crystal must be a single crystal free from dislocations and that it must contain an infinitesimal amount of dopant and oxygen in respectively prescribed concentrations. For growing dislocation-free crystals, it is indispensable to stabilize the flow of the silicon melt in crucibles and, for regulating concentrations of the microelements in the crystal, it is imperative to control mass transfer from the melt to a crystal growth boundary.

Controllability of a melt is generally governed by its kinetic viscosity and the size of the vessel. However, silicon melt has as small a kinetic viscosity as only 1/10 that of water and 1/2 that of molten iron, another molten metal, and, for this reason, it is a difficult material to control. Over the last 20 years, the size of silicon crystal grew from 3" to 8", a 10-fold increase in terms of crucible capacity, and it has become clear, as a result of analyses through observations and numerical simulations during the course of the change, that flow behavior of the melt did not change in continuous proportions to the crucible size but did involve several qualitative changes in the form of flow.

With this as a background, Nippon Steel and NSC Electron undearstand that the melt flow behavior in the crystal making process is one of the key subjects in the developing to the 12" diameter

*1 Technical Development Bureau

crystal. These companies have examined changes in the melt flow characteristics through temperature measurements in commercial furnaces and numerical simulations of the flow and, based on their results, promoted researches to clarify the flow phenomena and work out flow control methods to cope with the phenomena. This report describes the silicon melt flow phenomena in crucibles clarified through the direct measurement of melt surface temperature and the authors developed non-stationary 3-dimensional numerical simulations.

2. Melt Flow during Crystal Growth

Most silicon single crystals for semiconductor devices are presently grown by the Czochralski (CZ) process[1], wherein a seed crystal is dipped into a raw material of molten silicon in a crucible and the silicon crystal grows while the seed crystal is slowly pulled upward and cooled (see **Fig. 1**). The process characterizes in that the crucible and the crystal rotate in reverse directions to each other on a common axis for the purpose of homogeneous heating and controlling the melt flow in the crucible. Since silicon melt is highly electrically conductive, it is also possible to control its flow through the Lorentz force by application of a magnetic field, as practiced in the casting of metals[2]. Thus, a torpedo-shaped and dislocation-free silicon single crystal is grown through precisely controlling rotations of the crystal and crucible, temperature of the melt and magnetic field, if applied.

Many of past technical papers on the crystal growth explained the melt flow in a vertical section on an assumption that the melt flow in the CZ process was axi-symmetric[3-7]. Those papers explained convection in crucibles as a product of multiple combinations of thermal convection induced vertically along the crucible wall by heating (free convection) with forced convection in a vertical section of the crucible caused by the rotations of the crystal and the crucible.

Several points about the axi-symmetric model are, however, open to arguments. In the first place, the silicon melt in the CZ process is unstable in terms of potential energy since it is heated from below and, for this reason, its internal flow cannot always be axi-symmetric, however axi-symmetrically the crucible may be positioned in relation to its heater. Further, it is true that angular momentum of the melt is conserved if the crucible rotates at a constant rate, but the thermal convection and the forced convection in a vertical section of the melt are rotational movements acting against the conservation of angular momentum. Hence, it is doubtful if or not the axi-symmetric convection movements can represent dominant flow of the melt. In the actual field practice of the crystal manufacture, plant operators know quite well from uneven radiation intensity from the melt surface that temperature distribution at the melt surface is not axi-symmetric but it is in a mesh pattern[8].

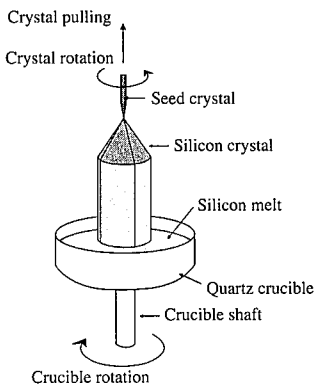

Fig. 1 Outline of crystal growth by CZ process

Facing these arguments, around the 1990s, many researchers began to approach the issue through temperature measurements of the melt and numerical simulations. The facts described below have been made clear about the melt flow, despite difficulties in the flow measurement because the melt is not being transparent and being placed in a vacuum and more than 1,400°C hot.

3. Measurement of Melt Flow

In the late 1980s, Kakimoto et al. initiated video image observation of trajectories of tracer particles planted in a silicon melt using an X-ray radiography trained on a commercial crystal growing furnace[9]. It was made clear for the first time by the observation that the tracer particles moved more in a horizontal sectional plane than they did in a vertical sectional plane by convection and that the melt flow was a complicated 3-dimensional movement. The above finding led to understandings that the melt flow was neither axi-symmetric nor laminar and that it was inappropriate to discuss about it in terms only of movements in vertical planes. It was also made clear that the trajectories of the tracer particles changed, depending on the crucible rotation speed, from a nearly axi-symmetric pattern to a spiral pattern with undulations in the azimuth direction. It was suggested from this that changes of the crucible rotation speed triggered transitions of the flow pattern[10].

Almost at the same time, through multiple point temperature measurement with thermocouples of the melt in commercial furnaces and phase analyses of the data thus obtained, the authors discovered, so did Seidle et al., that there were temperature distributions having wave-like structure in horizontal sections of the melt (see **Fig. 2**)[11,12]. These results were in good agreement with characteristics of the so-called "baroclinic waves" [13] and "Küpper-Lorts instability[14]," phenomena unique to thermal convection in a rotating system. The former is the essence of high-low pressure wave of the global atmosphere (see **Fig. 3**) and the latter is an instability phenomenon caused by the Bénard convection in a rotating system.

In 1996 the authors developed a device for real-time visualization of temperature distribution at the melt surface in order to observe the melt flow more in detail. By catching radiation energy from the melt surface with a CCD video camera and converting it into temperature, the device is capable of collecting temperature distri-

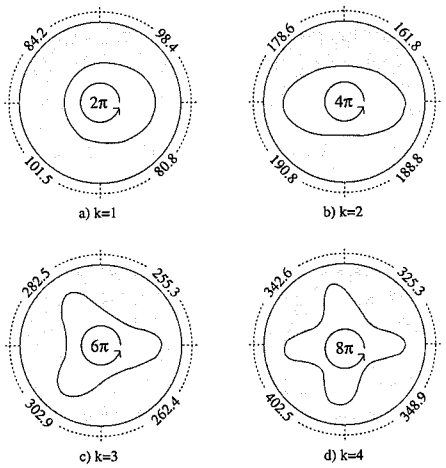

Fig. 2 Temperature fluctuation modes of melt surface calculated from phase analysis (Numerical figures show phase differences of temperature fluctuation among four measurement points)

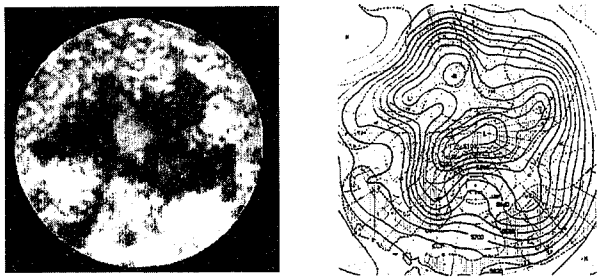

a) Temperature distribution of CZ melt surface measured with CCD

b) Distribution of isobaric altitudes of 500 mb and isotherms of global atmosphere

Fig. 3 Baro-clinic wave in CZ melt and global atmosphere

Fig. 4 Change in temperature distribution of melt surface measured with CCD camera under different crucible rotations (Downward view of melt surface center from top of crystal pulling furnace)

bution data of 768 × 493 pixels at an interval of 1/30 sec. and accuracy within 1°C. The data are recorded in the form of video images and it is possible also to trace historical temperature change at any chosen pixel[15].

Fig. 4 shows temperature images of the melt surface observed in a crucible 22" in diameter. Fig. 4 a) is an example of a slowly rotating crucible, where a temperature distribution is seen in an n-fold axi-symmetric spoke-like pattern. When the crucible rotation was 5.0 rpm or faster, an island pattern of high temperature cells appeared as shown in Fig. 4 c). With a crucible rotation ranging from 0.3 to 5.0 rpm, the n-fold axi-symmetric spoke-like pattern ((b1) of Fig. 4 b) and the island pattern ((b2) of Fig. 4 b) were observed to appear by turns, showing that the melt flow was changing more unstably than suspected. The characteristics of the melt flow as described above can be made clear through the Fourier analysis and wavelet analysis[16] of the time fluctuation data of each pixel temperature. It has been clarified from a wavelet analysis of the temperature fluctuation shown herein that the following three flow modes were involved: 1) a periodical fluctuation in synchronization with the crucible rotation and lasting for a considerably long period; 2) a single frequency fluctuation appearing chaotically; and 3) a slow fluctuation independent from the crucible rotation (see **Fig. 5**).

Further, it is possible to catch changes in statistic characteristics of turbulence from the shape of the power spectrum obtained through the Fourier spectral analysis. When rotating speed of a slow-rotating crucible with an island pattern is accelerated, the gradient of the spectrum becomes larger and it is possible to see degree of freedom of the turbulence is restricted by the crucible rotation. When the rotation rate is high enough, the spectrum gradient is seen to coincide with the frequency to the –4th power (see **Fig. 6**)[17]. This indicates that only the vertical component of the melt flow is restricted and the flow becomes turbulent only in two directions in a horizontal plane(2-dimensional turbulence). This state is known as the geostrophic tur-

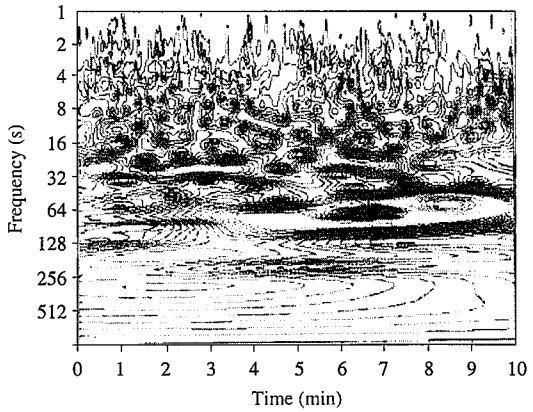

a) Temperature fluctuation characteristics at melt surface center

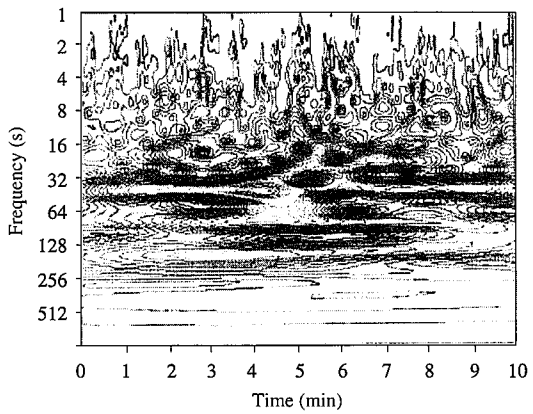

b) Temperature fluctuation characteristics at 74 mm away from melt surface center

Fig. 5 Wavelet analysis of time series data from CCD temperature measurement (Contour lines show magnitude of converted wavelet values)

bulence in rotating vessels. The vortices seen on the outer surface of the Jupiter atmosphere are typical examples of the geostrophic turbulence (see **Fig. 7**). It has been recorded lately, further, how the turbulence is amplified by application of magnetic fields[18].

Thus, as the observation of the actual melt advanced, it became clear that the conventional axi-symmetric model did not reflect the real phenomenon. The fact that there are complicated movements on the melt surface in the CZ process points out that the transfer of heat and substances(oxygen, dopant) from the crucible periphery toward the center is greatly influenced by not only the convection in vertical sections but also fluctuation of the flow in horizontal planes. From the above historical background it became necessary to view the flow of silicon melt from a new standpoint, namely, to look at the phenomena from a viewpoint inside a system of coordinates that rotates with the crucible, wherein the crucible rotation is regarded as a factor not to stir the melt but to change its state of flow through the Coriolis force.

4. Work of Coriolis Force

In a system of coordinates that rotates together with a crucible, equation of the melt motion is expressed as Eq. (1) where the effect of the crucible rotation is included as the Coriolis force.

$$\frac{\partial \mathbf{u}}{\partial t} + (\mathbf{u}\cdot\nabla)\mathbf{u} = -2(\Omega\times\mathbf{u}) - \frac{\nabla P}{\rho} + \alpha\mathbf{g}T + \nu\nabla^2\mathbf{u} + \frac{\sigma}{\rho\mu}\mathbf{J}\times\mathbf{B} \qquad (1)$$

where ρ is density, Ω: angular velocity vector of the crucible rotation, α: volume expansion coefficient, P: pressure, **g**: gravitational

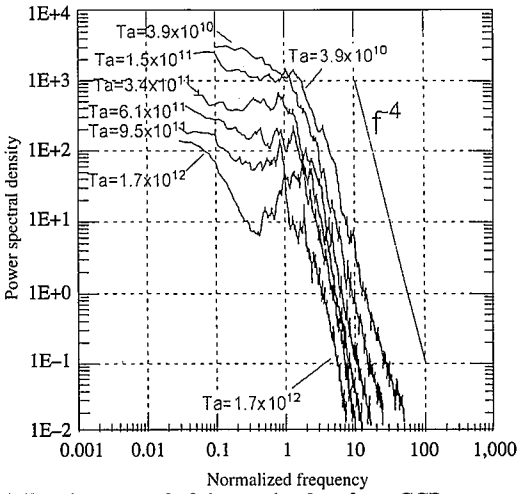

Fig. 6 Fourier spectral of time series data from CCD temperature measurement

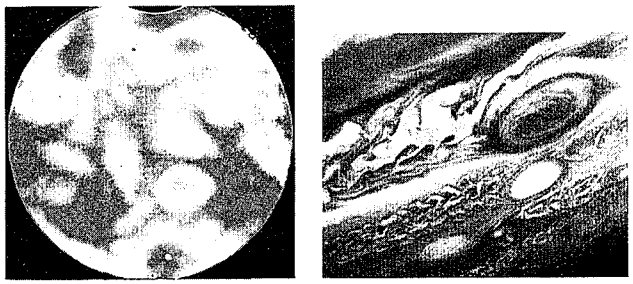

a) Temperature distribution at CZ melt surface by CCD temperature measurement

b) Vortices near the Great Red Spot of the Jupiter atmosphere

Fig. 7 Geostrophic turbulence in CZ melt and Jupiter atmosphere

acceleration vector, ν: kinetic viscosity coefficient, **u**: flow velocity vector, T: temperature, **J**: vector of induction current, **B**: vector of applied magnetic field, and σ: electric conductivity.

Table 1 roughly compares the forces acting on the CZ melt estimated by Eq. (1) from material characteristic figures of silicon, observed flow velocity and temperature, and intensity of the applied magnetic field.

Here, it can be seen that in the CZ melt the flow phenomenon is governed by the balance of buoyancy force, inertial force and Coriolis force and that the viscous force is negligibly small. It is therefore meaningless to discuss about the melt flow characteristics in terms only of conventionally used values relative to viscosity such as the Rayleigh number (buoyancy force/viscosity force) and the Reynolds number (inertial force/viscous force) and it becomes necessary to use dimensionless numbers including the Coriolis force as indicators for explaining the phenomena occurring in the CZ melt. The Taylor number (T_a) and Rossby number (R_o) are examples of such dimensionless numbers, and they are defined as follows, respectively:

$$T_a = \frac{4\Omega^2 R^4}{\nu^2} = (\text{Coriolis force/viscous force})^2 \qquad (2)$$

Table 1 Comparison of forces acting on CZ melt in crucible

Forces acting on melt	Term in Eq. (1)	Relative magnitude
Inertial force	2nd term in left	1
Coriolis force	1st term in right	1
Buoyancy force	3rd term in right	10
Viscosity force	4th term in right	1/10,000
Lorentz force	5th term in right	0 - 10

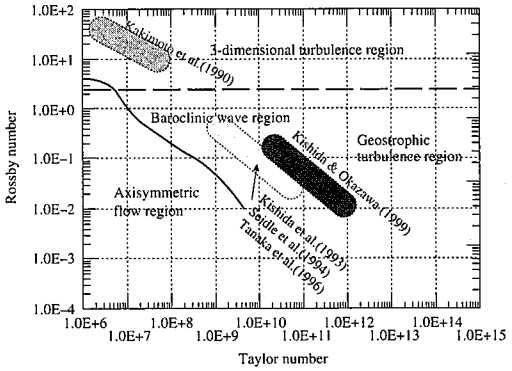

Fig. 8 Thermal convection regime and CZ silicon melt conditions in rotating system

$$R_o = \frac{U}{2\Omega R} = (\text{inertial force/Coriolis force}) \qquad (3)$$

where Ω is rotation of the crucible, R: a typical length (radius) of the crucible, and U: a typical flow velocity of the melt.

Generally speaking, the following three are counted as effects of the Coriolis force: 1) to make curvature of the flow larger; 2) to restrict convection movements; and 3) to stabilize the flow. Influence of these effects on the thermal convection of the melt flow is complicated. Luckily, however, investigations of similar phenomena are well advanced through studies of global atmospheric and oceanographic dynamics, and the knowledge accumulated through these studies have served to the study of the CZ silicon melt flow.

For instance, there are many researches to explain thermal convection in a rotating system by the Rossby number and the Taylor number shown in Eqs. (2) and (3) using the Coriolis force as an indicator, and phase diagrams such as the one shown in **Fig. 8** have been worked out through theoretical calculations and experiments[19]. According to the phase diagram, form of the thermal convection in a rotating system is classified into 3-dimensional turbulence, baro-clinic wave and geostrophic turbulence, depending on the distribution of the Coriolis force, inertial force and viscous force. Fig. 8 also shows the conditions corresponding to the observations of the CZ silicon melt reported so far. It can be seen in the figure that, whereas in small laboratory crucibles around 3" in diameter the melt flow tends to form a 3-dimensionally structured and unstable thermal convection, in large industrial crucibles over 10" the flow becomes turbulence, etc. due to a large amount of Coriolis force. Further, because of the small kinetic viscosity of silicon melt, the flow condition does not fall within the axi-symmetric flow region in the lower left area of Fig. 8. Although the conditions assumed in the phase diagram do not perfectly meet the conditions of the CZ silicon melt, the melt characteristics obtained from experiments on actual melts fit well into the flow classifications in the phase diagram. Thus, we may well say that what happen in the CZ silicon melt are identical to the baroclinic wave of the high-low pressure wave of the global atmosphere and the geostrophic turbulence seen in the Jupiter atmosphere. The chaotic temperature fluctuation observed in the above-mentioned CCD measurement can be attributed to transitions between these states of flow.

5. Numerical Simulation

Many of early numerical simulations of the CZ melt flow were based on an assumption of a stationary state under a 2-dimensional axi-symmetric model. Results of the above-mentioned observations, however, called for analyses using 3-dimensional non-stationary

models. This seems to require quite a large computer capacity. In reality, however, it is possible to reproduce phenomena reflecting those obtained through observations or experiments without drastically enhancing resolution of the models employed or using sophisticated turbulence models, because information of observations has clarified outlines of the flow structure. The reasons for this are described below.

In the first place, it is known that undulation of isotherms and vortex structure can be grasped from the CCD temperature measurement at a resolution of 1/10 that of the visual images by the CCD. It is also clear from X-ray observations that there is no large difference in intensity between horizontal and vertical movements of the flow. For reproducing the observed phenomena, therefore, a number of calculation lattice points in the order of several hundreds of thousands would be enough, i.e., 50 points along each of the horizontal axes and vertical axis. The memory capacity required for the calculation of the above number of lattice points will only be several hundreds of MB, a figure easily available with latest personal computers.

In normal flow calculations, applicability of a turbulence model is judged based on the value of the Reynolds number (ratio of inertial force to viscous force). But, since the Reynolds number of the CZ melt flow is in the order of 10^7, a stable calculation is judged impossible with 500,000 or so of lattice points, unless a turbulence model is introduced[20]. In the CZ melt where the Coriolis force largely contributes to stabilizing the flow, however, the fact that the Coriolis force is comparable to the inertial force works favorably and stable calculation is possible with 500,000 or so of lattice points, not bothering to use a turbulence model.

Thus, the Coriolis force makes stable calculation viable, but this brings about problems, too. For example, the Coriolis force forms the Eckman boundary layer and the Stewartson boundary layer on the inner surface of the crucible[13] and this causes the thickness of the boundary layer thinner than in simple viscosity models, and this requires that the lattice points have to be chosen carefully. As seen in the CCD temperature measurement images, some boundaries at the silicon melt surface between low and high temperature zones are clearly seen like junction lines of ocean currents. Because there is a large difference in velocity there, the inertial force is locally large and it is necessary to apply higher order difference models[21] in digitizing the inertia term of Eq. (1).

In actual calculations, temperature distributions close to observation results, as described below, can be obtained even using rough models with simplified crucible shape and boundary conditions[14,15].

Figs. 9 and 10 show results of a series of calculations under a condition where the Coriolis force was changed while maintaining the buoyancy force acting on the melt. Temperature distribution is shown here in isotherms at the surface and a vertical section of the melt. In the calculation model used therein, the crucible is cylindrical, the temperature distribution of the crucible side wall is given in a fixed value, and the temperature gradient at the melt surface is determined in accordance with the heat flux defined by the radiation under an atmosphere temperature of 1,525K. Fig. 9 shows the calculation results in the ascending order of the Coriolis force in columns (A) to (C). The figures in each of the columns are, from the top to the bottom, the temperature distribution and flow trajectory at the surface, and the temperature distribution and flow trajectory at a vertical sectional plane including the crucible centerline. The figures are the images viewed from a point included in the coordinate system rotating together with the crucible and, thus, the velocity component

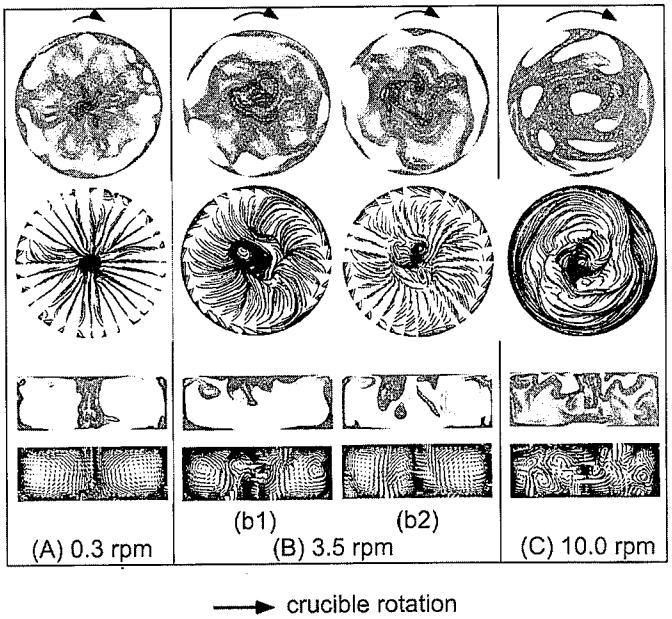

Fig. 9 Results of CZ silicon melt flow simulation - with small influence of Coriolis force

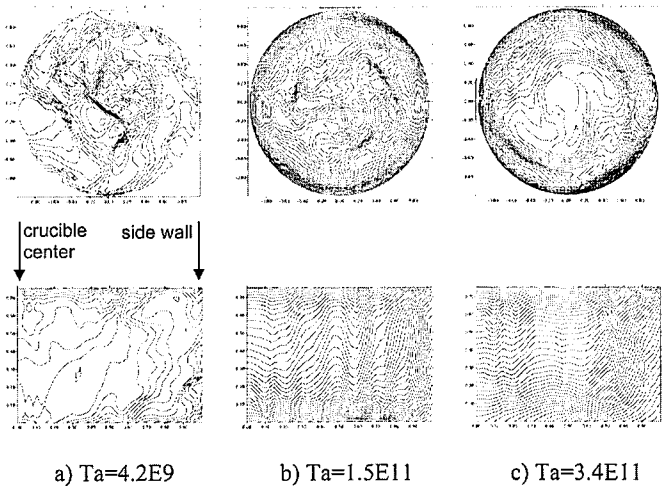

Fig. 10 Results of CZ silicon melt flow simulation - with large influence of Coriolis force (Top: isotherms at melt surface; Bottom: isotherms at vertical cross section of melt)

corresponding to the rotation is subtracted from them. Because of the unsteady calculation used here, each of the figures shown in the figure is a snap shot caught at one moment of the changing phenomena.

In the condition of column (A) of Fig. 9, the Coriolis force is as small as only 1/5,000 of the buoyancy force. The trajectories in the vertical sectional plane show that the flow forms a large convection, creeping up from the crucible bottom along the sidewall and, once on the surface, converging towards the center and going down at the center. The trajectories in the horizontal plane show, on the other hand, that the flow coming up along the sidewall sinks while converging in straight lines towards the center. The portions where the downward flow is strong are distributed periodically in the peripheral direction, and the temperature is lower there. This corresponds to the spoke-like pattern and is not much different from our usual understanding of natural convection.

In the condition of column (B) of Fig. 9, the Coriolis force is

larger than in column (A) but it is yet as small as about 1/650 of the buoyancy force. The calculation results are mostly as shown in (b1) but sometimes takes the form shown in (b2). What is common to both the forms is that the hot currents creeping up along the sidewall to the surface flow towards the center in arc-like curves. For this reason, the hot portions cool down before reaching the center and sink to form a wide low temperature zone at the center of the crucible bottom. In (b1), the portions where the downward flow is strong are distributed periodically in the peripheral direction to form an n-fold pattern. In the pattern of (b2), which appears sometimes, high temperature zones are distributed in islands near the crucible center and there is a vortex in the surface plane. Under this condition, small as it is, the influence of the Coriolis force is clearly seen from the curved flow trajectories and the presence of vortex.

In the condition of column (C) of Fig. 9, the Coriolis force is larger yet than in column (B) to reach 1/250 of the buoyancy force. There is no large convection encompassing the entire interior of the crucible in the vertical plane, but the convection is divided into several cells. In correspondence to this, a characteristic pattern with dispersed high temperature zones appears on the surface. The curvature of the flow trajectories on the melt surface is tighter to form horizontal vortices, the centers of which coincide with the centers of the high temperature zones. It is suspected that this is because the hot portions boiling up from the bottom is prevented by the Coriolis force from spreading towards the periphery and they cool and sink near where they have surfaced up.

Calculations under conditions with yet larger values of the Coriolis force[17] yielded the results shown in Fig. 10. In the condition of column a) of Fig. 10, the Coriolis force is 1/70 of the buoyancy force. Looking at the temperature distribution at the melt surface, the island pattern is seen in only 2/3 of the entire melt surface near the center. In the vertical section, isotherms run near the sidewall almost in parallel to it, showing no signs of the heat from the crucible being transferred by convection. In addition, disorder of isotherms near the crucible center is smaller than any of Fig. 9.

In the condition of column b), the Coriolis force is 1/20 of the buoyancy force. In a horizontal section under this condition, isotherms are more tightly packed near the sidewall than column a), while vortices are smoothed down, with cold portions more widely spread in the central region. Looking at isotherms in a vertical section, they run at equal and tight intervals in parallel to the sidewall in the boundary region with it and they are nearly horizontal in the other regions.

It can be seen in these results that the stronger the Coriolis force, the more restricted vertical convection tends to be. Contribution ratios of vertical components to the total kinetic energy of the melt are plotted in relation to the Taylor number in **Fig. 11** based on the numerical calculations under different conditions. In the low Taylor number region, the kinetic energy is distributed evenly in any direction and the contribution of the vertical components is roughly 30%, but the contribution rapidly falls from around the point of a Taylor number exceeding 10^{11}, showing clearly that vertical movement is suppressed as the Coriolis force increases.

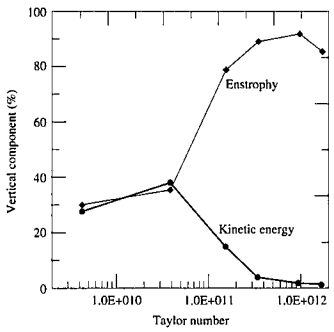

Fig. 11 Change of contribution ratios of vertical components to total kinetic energy of melt in relation to Taylor number by numerical simulation

6. Closing Remarks

This paper described, regarding melt flow during the CZ silicon crystal growth, that conventional axi-symmetric models were reviewed in consideration of observation results and that numerical simulations of the melt flow closer to the reality were made practicable by viewing the silicon melt flow from a standpoint in a system of coordinates that rotates together with the crucible. Flow analysis using numerical simulations tends to employ increasingly sophisticated turbulence models with highly condensed lattices, as available computer resources increase. But this study experiences into the CZ silicon melt flow seem to say that, before going into such sophistication, it is important to appropriately select a viewpoint for the approach to the phenomenon in question and study the real nature of the phenomenon into depths.

The numerical simulation of the CZ silicon melt flow is presently used as a tool for projecting process changes required by factors such as application of magnetic fields and scaling up of the crystal size. The time required for the projection is much longer than that for actually growing the crystals. In actual development activities under time restrictions, it is necessary to estimate possible mechanisms to explain actual phenomena based on analyses of data obtained from a limited number of calculation results. A full utilization of calculated data together with graphic expression of calculation results will contribute to optimization of flow control and creation of new ideas in the course of the scaling up of the crystal diameter.

Reference

1) Shimura, F.: Crystal Engineering of Silicon Semiconductor. Maruzen, Tokyo, 1993, p.44
2) Takasu, S., Ohwa, M., Suzuki, O., Higuchi, T: Oyo Buturi. 59 (8), 1044 (1990)
3) Hoshikawa, K., Hirata, H.: J. Appl. Phys. 60 (8), 808 (1991)
4) Kobayashi, N.: J. Jpn. Assoc. Cryst. Growth. 9 (1&2), 1 (1982)
5) Carruthers, J.R., Nassau, K. : J. Appl. Phys. 39, 11 (1968)
6) Langlois, W.E. : Ann. Rev. Fluid Mech. 17, 191 (1985)
7) Jones, A.D.W. : J.Crystal Growth. 88, 465 (1988)
8) Yamagishi, H., Fusekawa, I.: J. Jpn. Assoc. Cryst. Growth. 17, 42 (1990)
9) Watanabe, M., Eguchi, M., Kakimoto, K., Baros, Y., Hibiya, T. : J. Crystal Growth. 128. 288 (1993)
10) Kakimoto, K., Eguchi, M., Watanabe, M., Hibiya, T. : J. Crystal Growth. 102, 16 (1990)
11) Kishida, Y., Tanaka, M., Esaka, H. : J. Crystal Growth. 130, 75 (1993)
12) Seidl, A., McCord, G., Muller, G., Leister, H.J. : J. Crystal Growth. 137, 326 (1994)
13) Greenspan, H.G. : The Theory of Rotating Fluids. Cambridge Univ. Press, Cambridge, 1968. p.293
14) Boubnov, B.M., Golitsyn, G.S. : Convection in Rotating Fluids. Kluwer Academic publishers, Dordrecht, 1995, p.39
15) Tanaka, M., Hasebe, M., Saito, N. : J. Crystal Growth. 180, 487 (1997)
16) Chui, C.K. : An Introduction to Wavelets. Academic Press, Boston, 1992, p.49
17) Kishida, Y., Okazawa, K. : J.Crystal Growth. 198/199, 135 (1999)
18) Kishida, Y., Tamaki, T., Ohashi, W., Hasebe, M.: Proc. Symp. Jpn. Assoc. Appl. Phys. Spring, 1999, p.304
19) Fein, S., Pfeffer, R.L. : J. Fluid Mech. 75(1), 81 (1982)
20) Ferziger, J.H., Peric, M. : Computational Methods for Fluid Dynamics. Springer-Verlag, Berlin, 1996, p.249
21) Kawamura, T., Kuwahara, K. : AIAA Paper, 84 0340, 1984